Electronic Supplementary Information for

A [3Cu:2S] Cluster Provides Insight into the Assembly and Function of the Cu_Z Site of Nitrous Oxide Reductase

Lin Zhang,[a] Eckhard Bill,[b] Peter M. H. Kroneck,[c] and Oliver Einsle*[,a]

[a] *Institut für Biochemie, Albert-Ludwigs-Universität Freiburg, Albertstrasse 21, 79104 Freiburg im Breisgau, Germany.*

[b] *Max-Planck-Institut für Chemische Energiekonversion, Stiftstr. 34-36, D-45470 Mülheim an der Ruhr, Germany*

[c] *Fachbereich Biologie, Universität Konstanz, 78467 Konstanz, Germany.*

* *einsle@biochemie.uni-freiburg.de*

MATERIALS AND METHODS

Generation of expression constructs

Bacterial strains, plasmids and primers used in this study are listed in Tables S1. A FastCloning[1] protocol was used for site-directed mutagenesis of the seven histidine residues (H129A, H130A, H178A, H326A, H382A, H433A and H494A) of NosZ, and carried out based on plasmid pET22-nosZL(P).[2] The primers used are as follow: Primers ZL281/ZL282 were used to create variant H129A, primers ZL281/ZL282b for variant H130A, primers ZL283/ZL284 were used for variant H178A, primers ZL269/ZL270 to create variant H326A, primers ZL285/ZL286 for variant H382A, primers ZL287/ZL288 for variant H433A, and primers ZL289/ZL290 were used to create variant H494A.

Protein expression and isolation

Chemically competent cells of *E. coli* BL21 (DE3) strain C43[3] were transformed with the expression vectors, pET22-nosZL(P) and pET30-nosDFY(P) for protein production. Bacteria were grown at 37 °C to an OD_{600} of 0.6 in 2×YT medium supplemented with 100 $\mu g \cdot mL^{-1}$ ampicillin and 50 $\mu g \cdot mL^{-1}$ of kanamycin. Isopropyl-β-*D*-1-thiogalactopyranoside (IPTG) was added to a final concentration of 1mM to induce gene expression, and 0.25 mM $CuSO_4$ were supplemented for copper site maturation in over-expressed NosZ proteins. After further cultivation at 30 °C for 12 h with reduced agitation at 100 rpm, the cells were harvested by centrifugation for 15 min at 5,000×*g*. The cells were resuspended in lysis buffer (100 mM Tris/HCl buffer at pH 8.0, 150 mM NaCl and 10% (*v*/*v*) glycerol) and disrupted by ultrasonication (Branson Digital Sonifier 250) at 70% amplitude for 10 minutes (3 s working, 10 s pause). The crude extract was cleared by centrifugation at 100,000×*g* for 1 h, and the supernatant was loaded onto a Strep-Tactin Superflow cartridge (5 mL bed volume, IBA). Target proteins were eluted with lysis buffer containing 5 mM *D*-desthiobiotin (IBA) and further separated by size-exclusion chromatography (Superdex S200 26/60, GE Healthcare) equilibrated in 20 mM Tris/HCl buffer at pH 8.0, 150 mM NaCl. Pure protein was concentrated by ultrafiltration, flash-frozen in liquid nitrogen and stored at –80°C until further use. Protein concentration was determined by the bicinchoninic acid method, using bovine serum albumin as a standard.[4]

UV-vis spectroscopy

UV-visible absorption spectra of purified proteins (0.1 mM in 20 mM Tris/HCl buffer at pH 8.0, 150 mM NaCl) were measured in an anoxic chamber (Coy labs) and recorded over the scan range 200-900 nm using a USB 4000 Spectrometer with USB-ISS-UV/VIS Integrated Sampling System (Ocean Optics). Oxidation of protein samples was achieved by potassium ferricyanide, the stepwise reduction of Cu_A was done by adding sodium ascorbate, then further with sodium dithionite.

Electron paramagnetic resonance (EPR) spectroscopy

EPR spectra were recorded at X-band (9.63 GHz) using a continuous-wave (CW) ELEXSYS E-500 EPR spectrometer (Bruker) with a standard cavity (ER4102ST) and an ESR-900 helium

cryostat (Oxford Instruments). 300 µL of ferricyanide-oxidized, ascorbate-reduced, or dithionite-reduced, recombinant *Ps*N_2OR variants with a concentration of 60 mg·mL^{-1} were filled into an X-band EPR tube and frozen in liquid nitrogen. The measurements were carried out at temperatures of 10K, 40 K or 60K and a microwave power of 0.2 mW, with a modulation amplitude of 7.46 G. EPR simulations were performed with esimX (Max-Planck-Institute for Chemical Energy Conversion).

Nitrous oxide reductase activity assay

The activity of purified N_2O reductase was determined spectrophotometrically with Ti(III)-reduced benzyl viologen[5] in an anoxic chamber at room temperature. 100 µM of benzyl viologen were reduced with 80 µM titanium citrate in 10 mM potassium phosphate buffer at pH 8.5, and subsequently 1 µM of purified N_2O reductase were added; for determining kinetic data of the H178A variant, 8 µM protein was used in order to reach the steady-state range even for low activities. The absorption of the reaction mixture was monitored at 578 nm for 2 mins, then the reaction was initiated by the injection of dissolved N_2O in a concentration range of 2.5 to 2500 µM. The solubility of N_2O in water was assumed as 25 mM at 1 atm, 25 °C.[6]

Crystallization and structure determination

Recombinant *Ps*N_2OR variants were crystallized by sitting drop vapor diffusion at 20 °C, using protein at a concentration of 0.1 mM (6.68 mg·mL^{-1}) in SEC buffer. Drops with a total volume of 0.6 µl with different protein:reservoir ratios (1:2, 1:1) were equilibrated against 50 µL of a reservoir solution containing 0.1 M *bis*-tris propane buffer at pH 8.5, 0.1 M sodium formate, 0.1 M sodium chloride, and 25% (*w*/*v*) of a medium molecular weight (MMW) polyethylene glycol mixture (PEG 2K, 3350, 4K and 5K MME) from a PEG Smears screen,[7] using automated crystallization drop-setting (Oryx Nano, Douglas Instruments). Single crystals were obtained in combination with micro-seeding within one week and diffracted to below 2 Å. 10 % (*v*/*v*) of 2,3-butane diol were mixed with reservoir solution as a cryoprotectant and the crystals were harvested in nylon loops for flash-cooling in liquid nitrogen prior to data collection. Datasets to better than 1.7 Å resolution were collected at the X-ray absorption edge of copper (9050 eV) and zinc (9700 eV) on beamlines X06SA or X06DA of the Swiss Light Source (Villigen, Switzerland) with an EIGER 16M (Dectris) or a PILATUS 2M-F detector. Diffraction data were processed with autoPROC.[8] The crystal structures of *Ps*N_2OR variants were solved by molecular replacement with Phaser,[9] using a monomer of *Ps*N2OR (PDB ID 3SBQ)[10] as a search model. Improvement of the initial model was carried out in cycles of refinement with REFMAC5[11] and phenix.refine,[12] manual rebuilding was done in COOT.[13] The quality of the structure was validated by MolProbity.[14] Data collection and refinement statistics are summarized in Table S3.

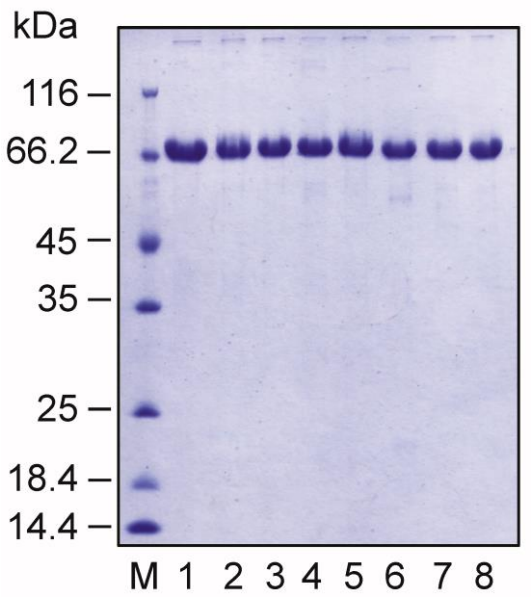

Figure S1. SDS-PAGE analysis of the variants. The molecular mass of C-termially Strep-tagged monomeric wild-type *Ps*N_2OR is 66.8 kDa. Protein samples (approximately 2 μg) loaded in each lane were: M, molecular weight marker; 1, wild-type; 2, H129A; 3, H130A; 4, H178A; 5, H326A; 6, H382A; 7, H433A; 8, H494A.

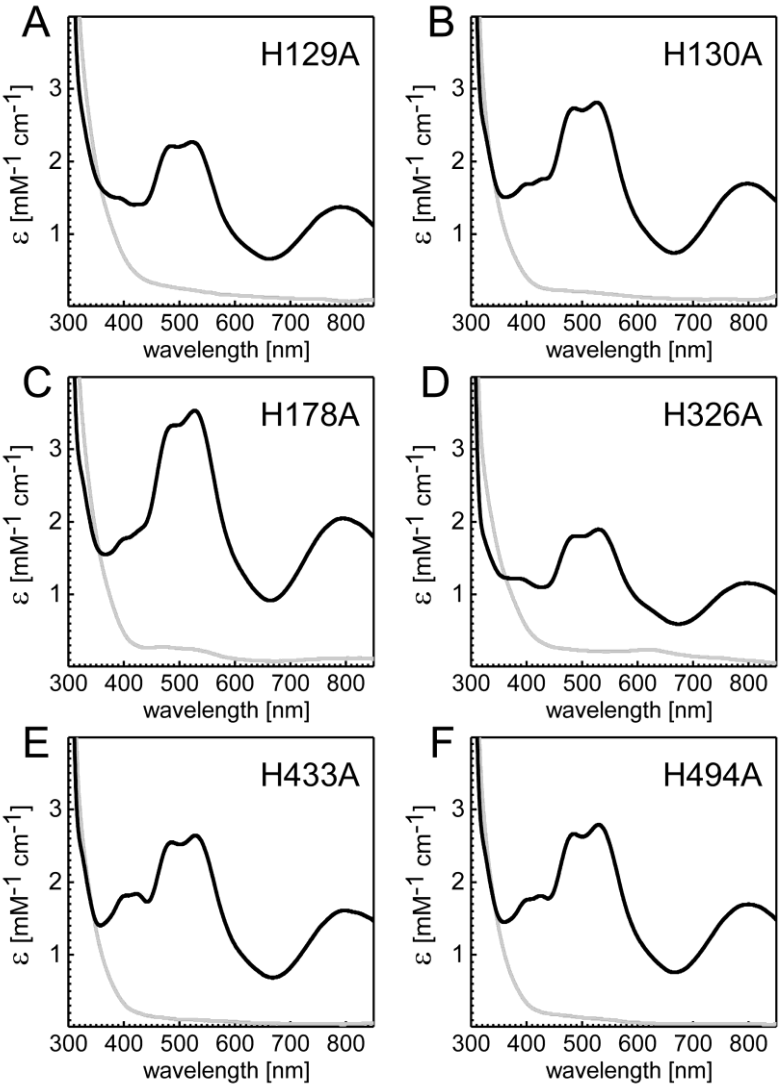

Figure S2. **UV-vis spectra of *Ps*N_2OR variants H129A (A), H130A (B), H178A (C), H326A (D), H433A (E) and H494A (F)**. The spectra of all the six variants upon oxidation with $K_3Fe(CN)_6$ (black curve) only show features for the Cu_A site (details in Table S2), and reduction with ascorbate (grey curve) eliminated the absorbance, therefore indicating the absence of a Cu_Z site. The absorption bands around 410 nm derive from excess oxidant.

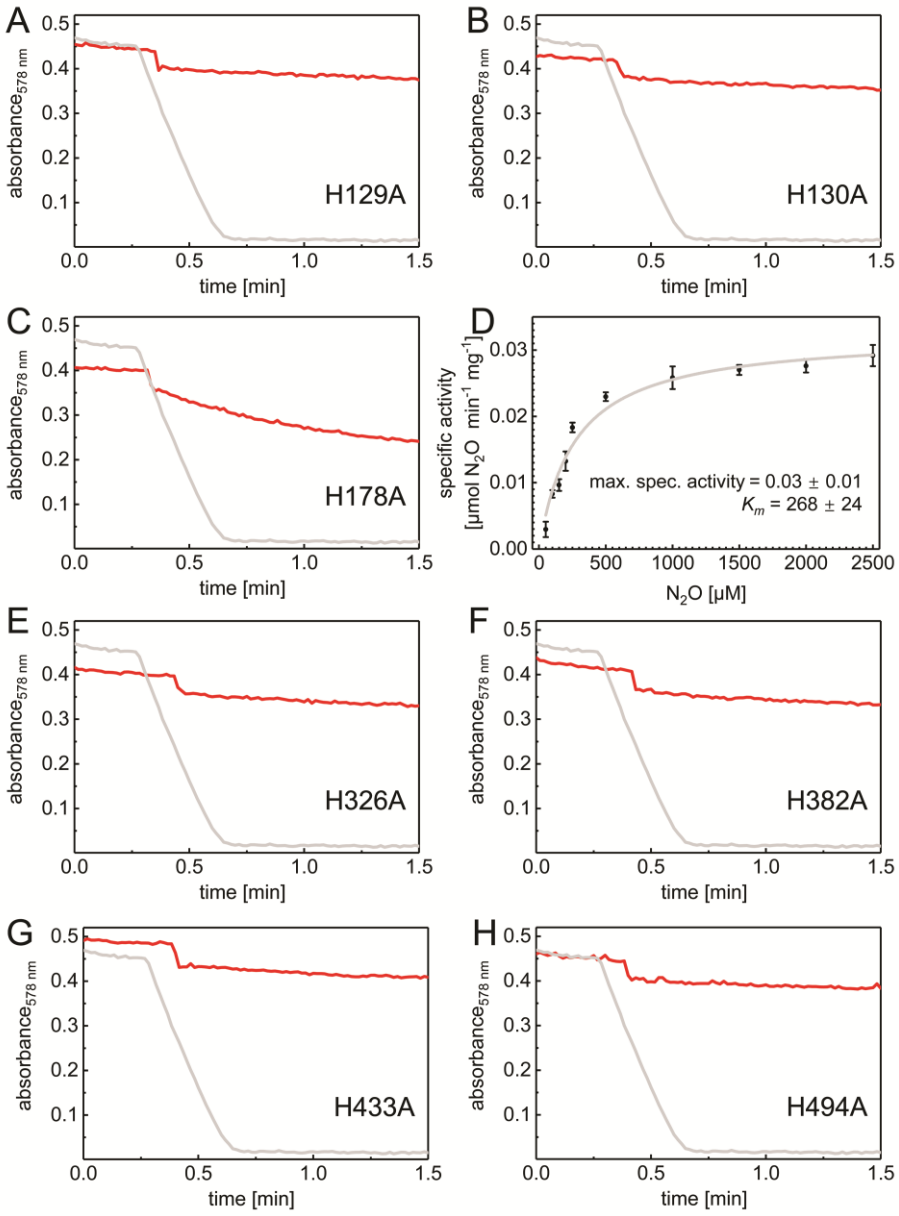

Figure S3. *In vitro* activities of the seven variants using benzyl viologen as an electron donor. The concentration of protein used in the assay was 1 μM; the N_2O concentration was 25 μM for wild-type N_2OR as a positive control (grey curve), and 2.5 mM for the variants (red curve). Six of the variants, namely H129A, H130A, H326A, H382A, H433A and H494A, showed no activity. Unexpectedly, H178A had low catalytic activity (C). A kinetic assay for H178A (D) showed very low specific activity (0.03 ± 0.01 μmol N_2O $min^{-1} \cdot mg^{-1}$) and a high K_M (268 ± 24 μM N_2O) value. The data were fitted with a Michaelis-Menten equation.

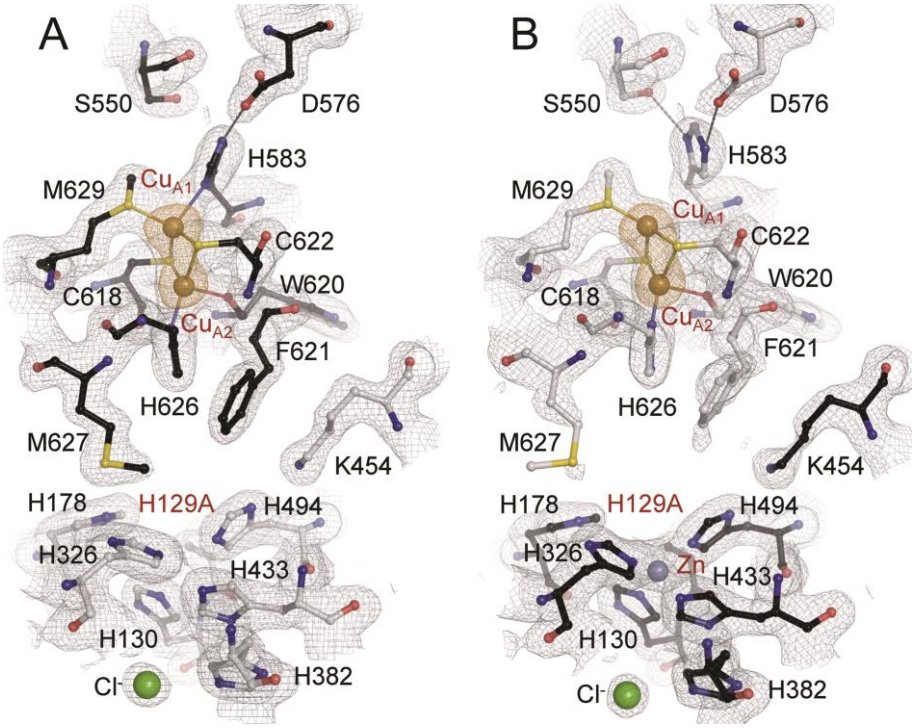

Figure S4. Three-dimensional structure of *Ps*N_2OR variant H129A. (A) Side A of the H129A dimer, which shows the Cu_A site of chain A and Cu_Z site ligands in chain B. Cu_A is intact and coordinated by H583, C618, W620, C622, H626 and M629. Residue H583 is in the bound conformation, ligating Cu_{A1}, and forms a short hydrogen bond to residue D576 (2.7 Å). The Cu_Z-binding site is depleted of any ligand. **(B)** Side B of the H129A dimer, with the Cu_A site of chain B and Cu_Z site ligands in chain A. The intact Cu_A is coordinated by C618, W620, C622, H626 and M629. However, residue H583 is in the unbound conformation and forms two hydrogen bonds to residue D576 (2.8 Å) and S550 (3.1 Å). No copper ion was observed in the Cu_Z site, but one Zn^{2+} ion was located, which coordinated by H130 (2.23 Å), H433 (2.54 Å) and H494 (2.01 Å). This was verified by analysis of the data collected at the X-ray absorption edge of Zn (9700 eV, data not shown). $2F_o–F_c$ electron density maps (grey) are contoured at the 1 σ level, and anomalous difference Fourier maps (orange) at the 6 σ level, highlighting the positions of copper ions.

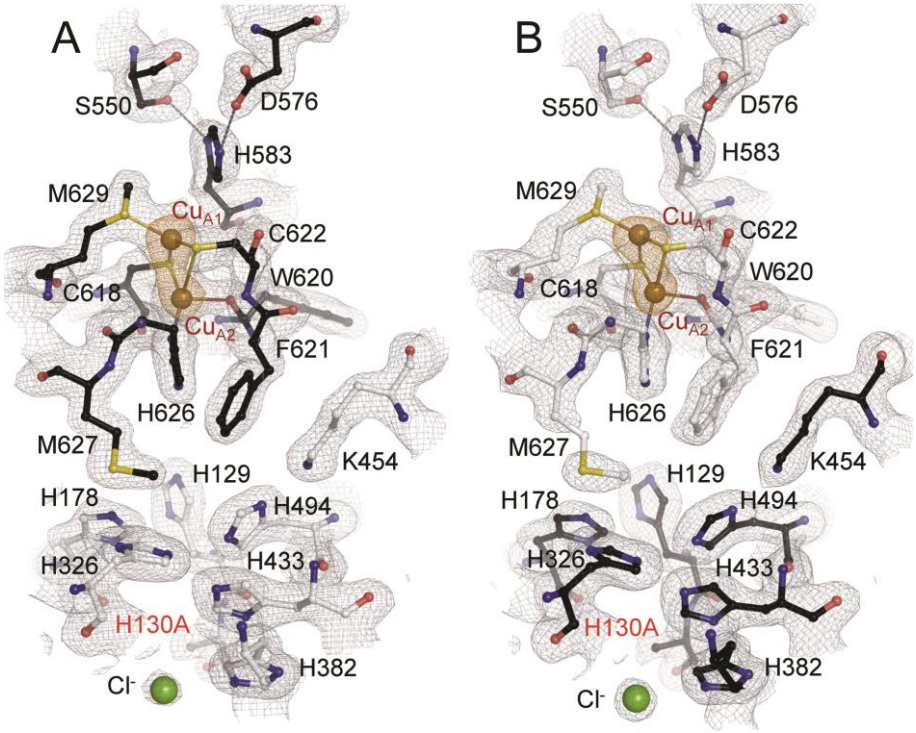

Figure S5. Three-dimensional structure of *Ps*N$_2$OR variant H130A. (A) Side A of the H130A dimer, showing Cu$_A$ in chain A and Cu$_Z$ site ligands in chain B. Cu$_A$ is coordinated by C618, W620, C622, H626 and M629, and residue H583 is in the unbound conformation, with hydrogen bonds to residue D576 (2.9 Å) and S550 (3.1 Å). No ligand was found in the Cu$_Z$ site. **(B)** Side B of the H130A dimer, with the Cu$_A$ site of chain B and Cu$_Z$ site ligands in chain A. Cu$_A$ has residue H583 in the unbound conformation, with hydrogen bonds to residue D576 (2.7 Å) and S550 (2.9 Å). No copper atom was found in the Cu$_Z$ site. $2F_o$–F_c electron density maps (grey) are contoured at the 1 σ level, and anomalous difference Fourier maps (orange) at the 6 σ level, highlighting the positions of copper ions.

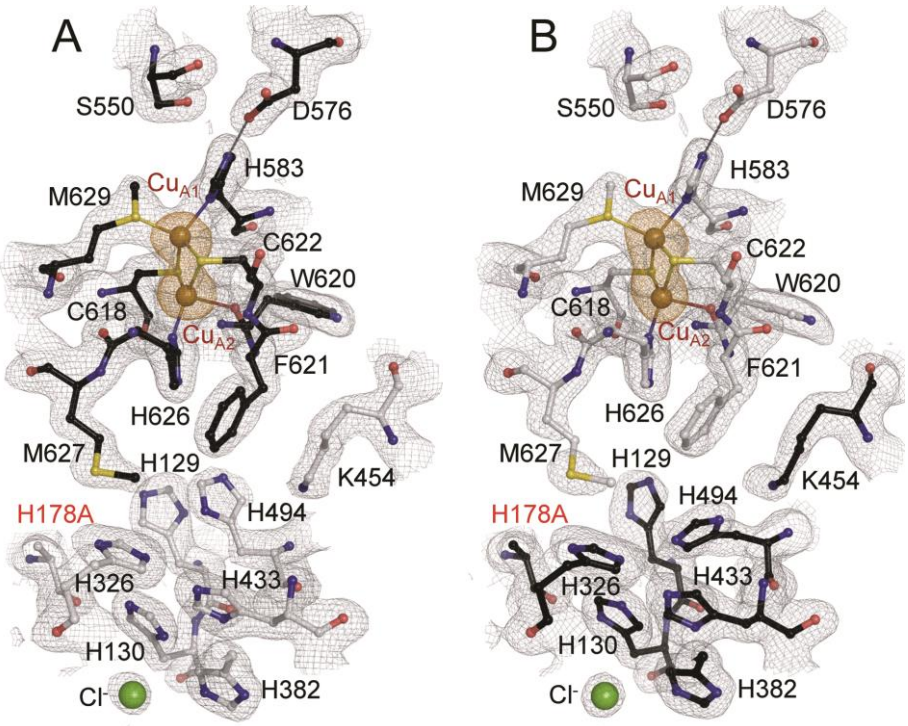

Figure S6. Three-dimensional structure of *Ps*N$_2$OR variant H178A. (A) Side A of the H178A dimer, with Cu$_A$ of chain A and the Cu$_Z$ site ligands in chain B. in the intact Cu$_A$ site, residue H583 is in the bound conformation, and forms a short hydrogen bond to residue D576 (2.6 Å). The Cu$_Z$ site is empty. **(B)** Side B of the H178A dimer, with the Cu$_A$ site in chain B and Cu$_Z$ site ligands in chain A. Cu$_A$ has residue H583 again in a bound conformation to ligate Cu$_{A1}$, and forms a short hydrogen bond to residue D576 (2.7 Å). No metal cation was observed in the Cu$_Z$ site. $2F_o$–F_c electron density maps (grey) are contoured at the 1 σ level, and anomalous difference Fourier maps (orange) at the 6 σ level, highlighting the positions of copper ions.

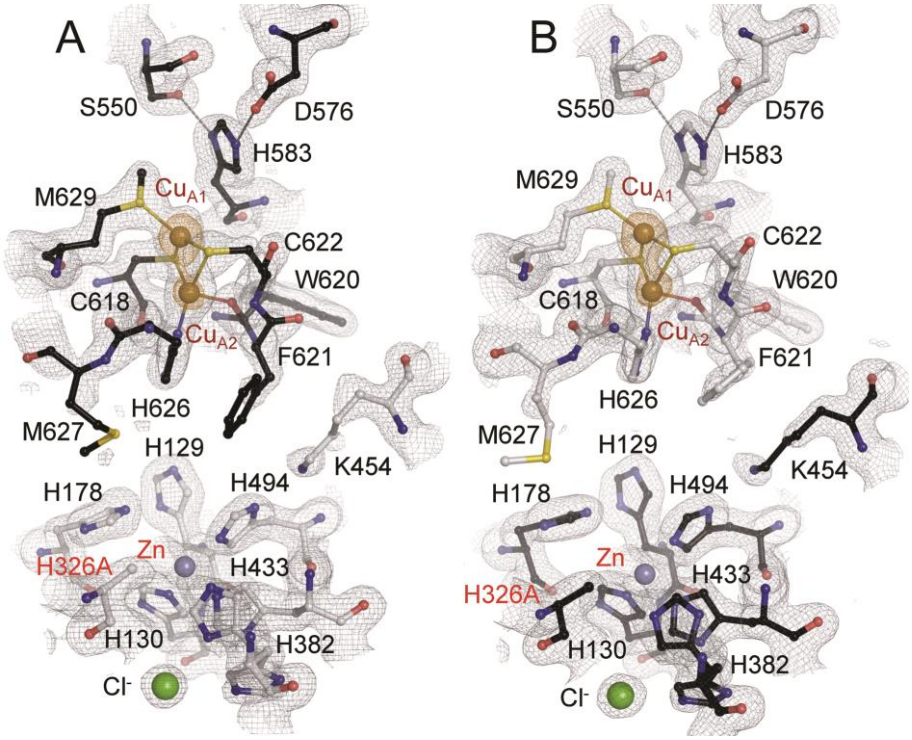

Figure S7. Three-dimensional structure of *Ps*N_2OR variant H326A. (A) Side A of the H326A dimer, with Cu_A in chain A and Cu_Z site ligands in chain B. The Cu_A site shows a significantly reduced occupancy, residue 583 is in the unbound conformation, forming two short hydrogen bonds to residues D576 (2.7 Å) and S550 (2.8 Å). **(B)** Side B of the H326A dimer, showing the Cu_A site of chain B and Cu_Z site ligands in chain A. Cu_A is present with low occupancy, and residue H583 is again in the unbound conformation with hydrogen bonds to residue D576 (2.7 Å) and S550 (2.8 Å). No copper ions were observed in in either sides in the Cu_Z site, but one Zn^{2+} bound to both chains, coordinated by H130 (2.22 Å, 2.16 Å), H433 (2.31 Å, 2.03 Å) and H494 (2.07 Å, 2.04Å). This was verified by data collected at the X-ray absorption edge of Zn (9700 eV, data not shown). $2F_o–F_c$ electron density maps (grey) are contoured at the 1 σ level, and anomalous difference Fourier maps (orange) at the 6 σ level, highlighting the positions of copper ions.

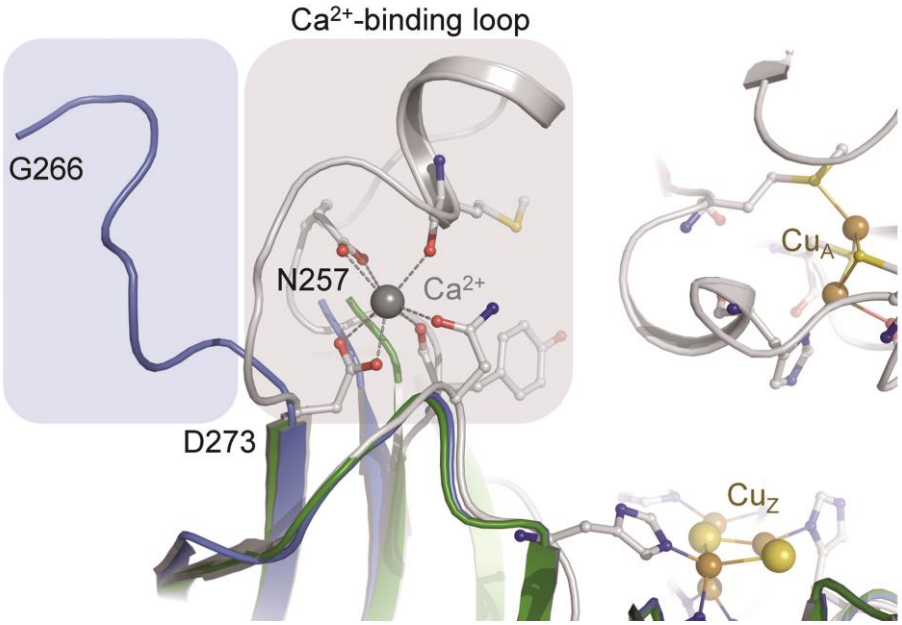

Figure S8. Alignment of the Ca^{2+}-binding loop of wild-type *Ps*N_2OR and variant H326A. After assembly of the copper site, the disordered loop between N257 and D273 closes into a fixed conformation by binding a calcium ion.[15] In the H326A structure, the Ca^{2+}-binding loops of both chains are disordered. Interestingly, the loop in chain B nevertheless is partially resolved (G266 to D273) due to crystal packing. This may also represent a physiologically relevant conformation during the assembly of the copper sites. The structure of wild-type *Ps*N_2OR (PDB code: 3SBQ) [16] is shown in grey cartoon, chain A of H326A is shown in green, and chain B in blue.

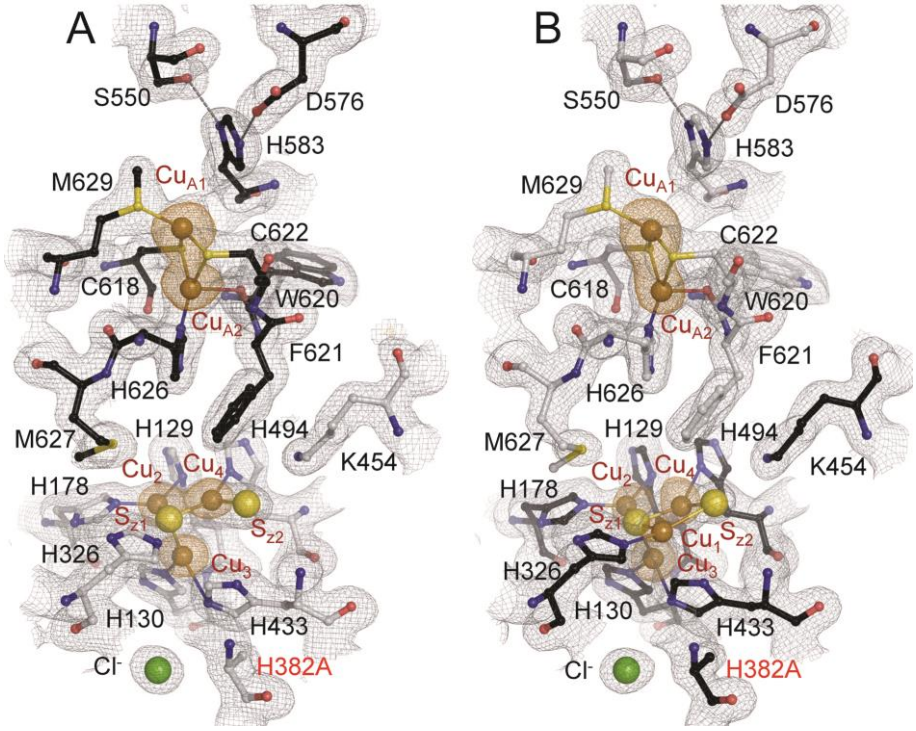

Figure S9. Three-dimensional structure of *Ps*N_2OR variant H382A. (A) Side A of the H382A dimer, with Cu_A in chain A and Cu_Z site ligands in chain B. Cu_A has residue H583 in its unbound conformation, with two hydrogen bonds to residues D576 (2.8 Å) and S550 (2.8 Å). Unexpectedly, three copper ions were observed in the Cu_Z site, namely Cu_{Z2}, Cu_{Z3}, and Cu_{Z4}, while Cu_{Z1} was absent. The site, however, still contains the edge sulfide S_{Z2} and thus comprises a [3Cu:2S] cluster. Futher details are shown in Figure 3. **(B)** Side B of the H382A dimer, showing the Cu_A site in chain B and Cu_Z site ligands in chain A. Cu_A has residue 583 in the unbound conformation with hydrogen bonds to residues D576 (2.8 Å) and S550 (2.7 Å). In contrast to side A, there is weak, residual density for Cu_{Z1}, modelled at 20% occupancy, while Cu_{Z2}, Cu_{Z3} and Cu_{Z4} were 50% occupied. Thus, we estimated the presence of 10% Cu_Z for the entire sample, providing an explanation for the UV-vis properties (Fig. 1F), where the sample can be slightly reduced further by dithionite after ascorbate reduction. The absence of activity can be rationalized such that without the coordination by residue H382 the residual Cu_{Z1} will not be sufficiently stable to support N_2O binding and reduction. $2F_o–F_c$ electron density maps (grey) are contoured at the 1 σ level, and anomalous difference Fourier maps (orange) at the 6 σ level, highlighting the positions of copper ions.

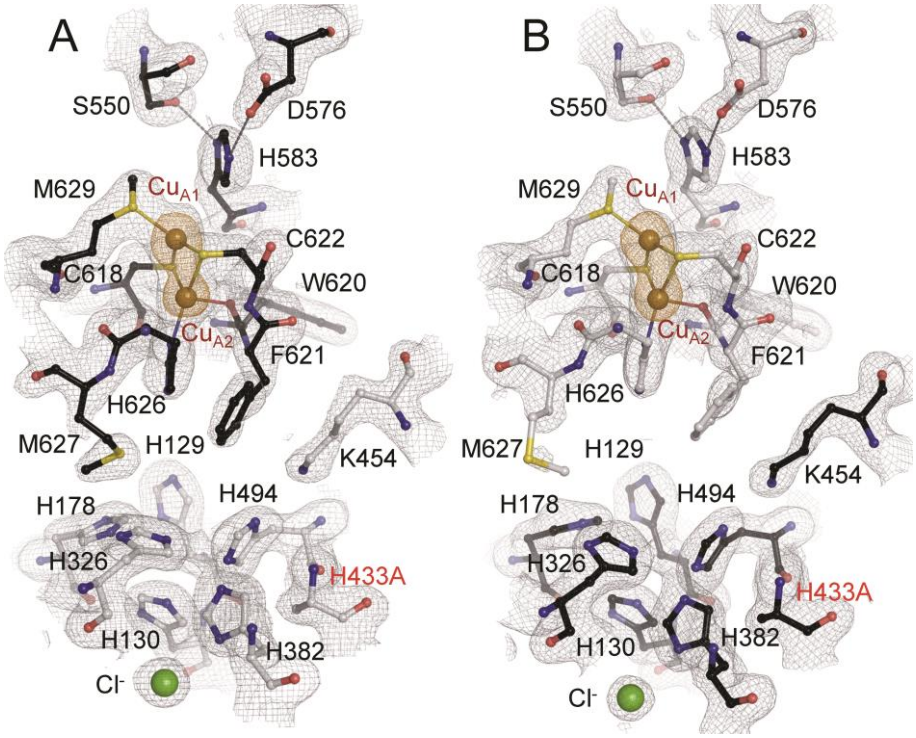

Figure S10. Three-dimensional structure of *Ps*N$_2$OR variant H433A. (A) Side A of the H433A dimer with the Cu$_A$ site of chain A and Cu$_Z$ site ligands in chain B. Cu$_A$ has residue H583 is its unbound conformation, with hydrogen bonds to residues D576 (2.9 Å) and S550 (3.1 Å). The Cu$_Z$ site is free of any ligands. **(B)** Side B of the H433A dimer, showing Cu$_A$ of chain B and Cu$_Z$ site ligands of chain A. Cu$_A$ has H583 in the unbound conformation, H-bonding to residues D576 (2.8 Å) and S550 (2.8 Å). The Cu$_Z$ site was ligand-free. $2F_o$–F_c electron density maps (grey) are contoured at the 1 σ level, and anomalous difference Fourier maps (orange) at the 6 σ level, highlighting the positions of copper ions.

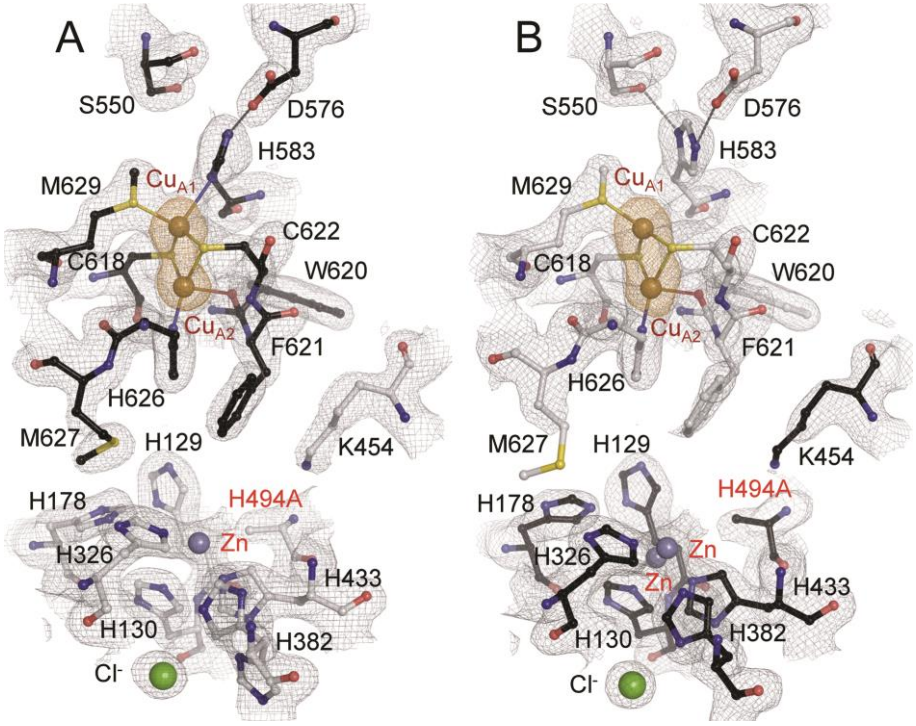

Figure S11. Three-dimensional structure of *Ps*N_2OR variant H494A. (A) Side A of the H494A dimer shows Cu_A in chain A and Cu_Z site ligands in chain B. Cu_A site has H583 in the bound conformation, forming a hydrogen bond to residue D576 (2.7 Å). No copper, but a single Zn^{2+} ion was found, coordinated by H326 (1.99 Å), H382 (2.18 Å) and H433 (2.99 Å). **(B)** Side B of the H494A dimer, with the Cu_A site in chain B and Cu_Z site ligands in chain A. In the Cu_A site, residue H583 is in the unbound conformation, H-bonding to D576 (2.8 Å) and S550 (2.9 Å). Uniquely, two Zn^{2+} ions were bound, coordinated by H130 (2.52 Å), H326 (1.98 Å), H382 (2.13 Å) and H433 (2.06 Å). This was verified by analysis of the data collected at the X-ray absorption edge of Zn (9700 eV, data not shown). $2F_o–F_c$ electron density maps (grey) are contoured at the 1 σ level, and anomalous difference Fourier maps (orange) at the 6 σ level, highlighting the positions of copper ions.

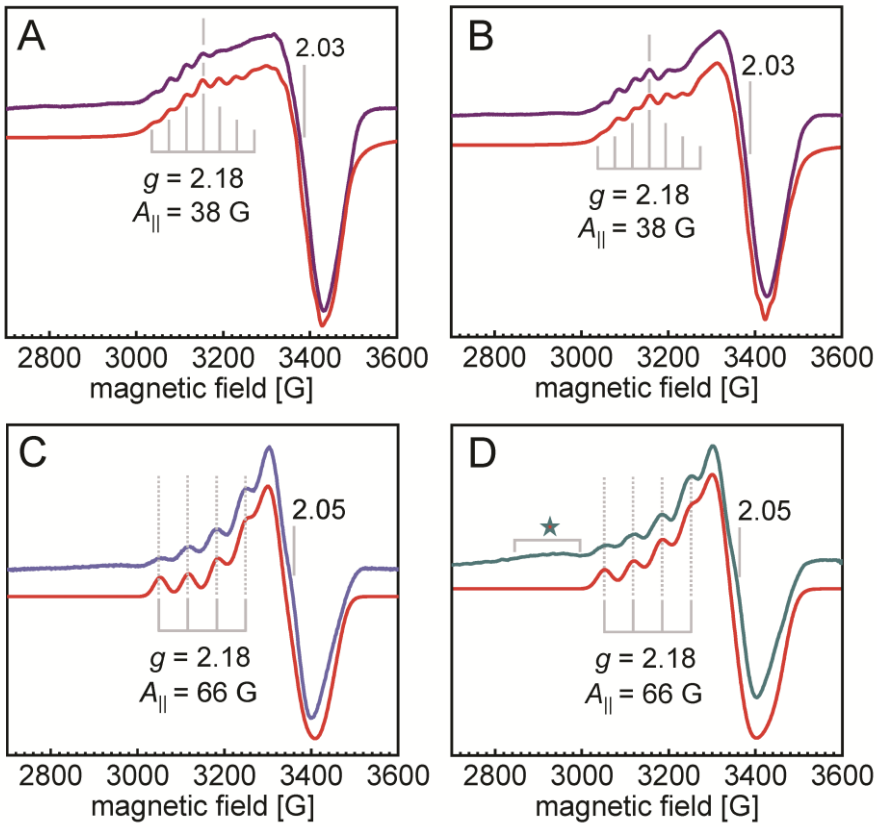

Figure S12. **Experimental and simulated X-band CW EPR spectra of WT *Ps*N_2OR (A) and variant H382A (B, C and D)**. For better visualization of the peaks, the intensities were not normalized. Spectra for ferricyanide-oxidized (purple), ascorbate-reduced (blue), and dithionite-reduced (cyan) samples are shown. Simulated spectra are shown in red traces. The region in panel D with star indicates the presence of free Cu^{2+} ion released from [3Cu:2S] site. The *g*-values used for simulations are *g* = (2.184, 2.039, 2.010) (A), *g* = (2.180, 2.037, 2.011) (B), *g* = (2.186, 2.053, 2.029) (C) and *g* = (2.186, 2.053, 2.029) (D), respectively. EPR simulations were performed with esimX.

Table S1. Bacterial strains, plasmids and primers used in this study.

Strains, plasmids and primers	Relevant characteristics	Ref. or sources
E. coli		
XL10-Gold	*endA1 glnV44 recA1 thi-1 gyrA96 relA1 lac Hte Δ(mcrA)183 Δ(mcrCB-hsdSMR-mrr)173 tetR F' [proAB lacIqZΔM15 Tn10(TetR Amy CmR)]*	Stratagene
C43(DE3)	*F– ompT gal dcm hsdSB(rB- mB-)(DE3)*	Lucigen
Plasmids		
pET22-nosZL(P)	*nosZLtatE* genes of *Pseudomonas stutzeri* in pET22b(+).	Previous work[2]
pET22-nosZL(P)H129A	with mutation in *nosZ* encodes H129A	This work
pET22-nosZL(P)H130A	with mutation in *nosZ* encodes H130A	This work
pET22-nosZL(P)H178A	with mutation in *nosZ* encodes H178A	This work
pET22-nosZL(P)H326A	with mutation in *nosZ* encodes H326A	This work
pET22-nosZL(P)H382A	with mutation in *nosZ* encodes H382A	This work
pET22-nosZL(P)H433A	with mutation in *nosZ* encodes H433A	This work
pET22-nosZL(P)H494A	with mutation in *nosZ* encodes H494A	This work
pET30-nosDFY(P)	*nosDFYtatE* genes of *Pseudomonas stutzeri* in pET30a(+).	Previous work[2]
Primer Names	Sequences	Descriptions
ZL281	5' - gcagtcaccgttgaggaac - 3'	
ZL282	5' - ttcctcaacggtgactgcgcgcacccgcacatctccatg - 3'	H129A
ZL282b	5' - ttcctcaacggtgactgccacgcgccgcacatctccatgacc - 3'	H130A
ZL283	5' - gatcgcctgcacgttcgg - 3'	
ZL284	5' - ccgaacgtgcaggcgatcgcgggtctgcgtctgcagaag - 3'	H178A
ZL269	5' - cgggtttttcggcactgg - 3'	
ZL270	5' - ccagtgccgaaaaacccggcgggctgcaacacctcctcc - 3'	H326A
ZL285	5' - cagcgggccgagacccag - 3'	
ZL286	5' - ctgggtctcggcccgctggcgaccaccttcgacggccgc - 3'	H382A
ZL287	5' - acccggctggtagtgcac - 3'	
ZL288	5' - gtgcactaccagccgggtgcgctgcacgcgtcgctgtgtg - 3'	H433A
ZL289	5' - cggttcggcaaaggtcgg - 3'	
ZL290	5' - ccgacctttgccgaaccggcggactgcatcatggctcgc - 3'	H494A

Table S2. UV-vis features for CuA from *Ps*N_2OR and variants

variants	λ_{max} (nm)[a]			extinction coefficient[b]			relative Cu_A occupancy[c]			
WT[d]	486	531	80	2.74	3.01	1.79	0.8	0.85	0.87	0.85 ± 0.03
H129A	486	523	79	2.21	2.27	1.38	0.6	0.64	0.67	0.66 ± 0.02
H130A	486	526	79	2.73	2.81	1.7	0.8	0.80	0.83	0.82 ± 0.02
H178A	488	527	79	3.33	3.53	2.05	1	1	1	1
H326A	485	529	79	1.8	1.9	1.16	0.5	0.54	0.57	0.55 ± 0.02
H382A	487	532	80	2.75	2.95	1.92	0.8	0.84	0.94	0.87 ± 0.06
H433A	486	528	79	2.55	2.64	1.61	0.7	0.75	0.79	0.77 ± 0.02
H494A	485	530	80	2.66	2.79	1.7	0.8	0.79	0.83	0.81 ± 0.02

[a] The spectra for Cu_A of WT and H382A were generated by subtraction of ascorbate reduced spectra (the contribution of Cu_Z site).

[b] The wavelengths of extinction coefficient values shown here are corresponding to the λ_{max}.

[c] All the other extinction coefficient values were normalized to that of H178A.

[d] Obtained from previously published data.[2]

Table S3. Data collection and refinement statistics.

Data sets	**H129A**	**H130A**	**H178A**	**H326A**	**H382A**	**H433A**	**H494A**
PDB accession code	6Y6Y	6Y71	6Y72	6Y77	7AQA	6Y7D	6Y7E
Space group	*P* 2_1	*P* 2_1	*P* 2_1	*P* 2_1	*P* 2_1	*P* 2_1	*P* 2_1
Cell constants a, b, c [Å]	69.46, 76.45, 108.45	69.16, 76.21, 109.02	68.74, 76.45, 108.76	69.84, 76.31, 108.45	68.82, 76.83, 108.51	69.30, 76.15, 108.20	69.28, 76.61, 108.46
α, β, γ [°]	90.00, 93.22, 90.00	90.00, 93.21, 90.00	90.00, 93.32, 90.00	90.00, 93.01, 90.00	90.00, 93.49, 90.00	90.00, 93.19, 90.00	90.00, 93.23, 90.00
Wavelength [Å]	1.36999	1.36999	1.36999	1.36998	1.36999	1.36999	1.36999
Resolution limits [Å]	76.45 – 1.67 (1.83 – 1.67)	76.21 – 1.64 (1.84 – 1.64)	76.45 – 1.55 (1.72 – 1.55)	76.31 – 1.49 (1.63 – 1.49)	108.3 – 1.50 (1.64 – 1.50)	76.15 – 1.60 (1.78 – 1.60)	108.3 – 1.60 (1.74 – 1.60)
Completeness (%)	95.2 (72.9)	94.3 (73.5)	94.8 (70.0)	95.2 (74.0)	86.6 (57.6)	94.9 (74.8)	91.7 (68.0)
Unique reflections	99132	90514	109991	135138	116124	101058	110732
Multiplicity (%)	6.6 (7.0)	6.6 (6.9)	6.6 (6.9)	6.7 (7.1)	7.4 (7.1)	6.4 (6.7)	7.0 (6.8)
R_{merge}[a]	0.077 (1.270)	0.099 (1.091)	0.048 (1.033)	0.085 (1.126)	0.065 (1.073)	0.080 (1.049)	0.067 (1.137)
$R_{p.i.m.}$	0.032 (0.518)	0.042 (0.445)	0.020 (0.424)	0.035 (0.453)	0.025 (0.426)	0.034 (0.435)	0.027 (0.465)
Mean I/σ (I)	15.4 (1.4)	11.6 (1.7)	21.8 (1.6)	13.7 (1.6)	15.9 (1.5)	12.5 (1.5)	15.3 (1.5)
$CC_{1/2}$	0.999 (0.590)	0.998 (0.660)	1.000 (0.684)	0.999 (0.629)	0.999 (0.669)	0.999 (0.671)	0.999 (0.624)
Refinement statistics							
R_{work}[b] / R_{free}	0.171 / 0.203	0.169 / 0.211	0.161 / 0.205	0.159 / 0.193	0.156 / 0.193	0.160 / 0.200	0.153 / 0.189
No. atoms	9992	10228	10358	10340	10393	10348	10333
Protein	9098	9244	9244	9065	9241	9145	9161
Ligand/ion	48	57	69	67	64	65	70
Water	846	927	1045	1208	1088	1138	1102
B-factor [Å^2]							
Protein	29.10	26.31	29.87	23.12	28.25	28.66	30.45
Ligand/ion	29.88	27.88	35.28	29.86	29.72	29.05	39.38
Water	37.90	33.43	39.51	35.03	39.66	37.79	43.01
R.m.s. deviations							
bond lengths [Å]	0.0071	0.007	0.0067	0.006	0.010	0.007	0.007
bond angles [°]	0.94	0.909	0.881	0.892	1.039	0.921	0.914

[a] $R_{merge} = \Sigma_{hkl} [(\Sigma_i |I_i - \langle I \rangle|) / \Sigma_i I_i]$

[b] $R_{work} = \Sigma_{hkl} ||F_{obs}| - |F_{calc}|| / \Sigma_{hkl} |F_{obs}|$; R_{free} is the cross-validation *R* value for a test set of 5 % of unique reflections.

Table S4. Bond lengths (Å) of the Cu_A sites in the seven variants.

variant	H129A		H130A		H178A		H326A		H382A		H433A		H494A		H583 conformation[a]	
chain	A	B	A	B	A	B	A	B	A	B	A	B	A	B	on	off
Cu_2-N_δ (H626)	2.20	2.21	2.21	2.25	2.15	2.13	2.33	2.25	2.14	2.11	2.24	2.11	2.22	2.14	2.18 ± 0.04	2.20 ± 0.07
Cu_2-O (W620)	2.43	2.54	2.39	2.43	2.49	2.54	2.51	2.62	2.47	2.41	2.46	2.54	2.52	2.64	2.50 ± 0.06	2.50 ± 0.08
Cu_2-S (C618)	2.58	2.65	2.56	2.57	2.58	2.64	3.02	2.72	2.79	2.81	2.83	2.83	2.75	2.70	2.64 ± 0.03	2.75 ± 0.14
Cu_2-S (C622)	2.70	2.60	3.30	2.93	2.50	2.59	2.68	2.70	2.63	2.62	2.74	2.75	2.63	2.59	2.61 ± 0.10	2.75 ± 0.22
Cu_2-Cu_1	2.70	2.71	2.70	2.71	2.67	2.69	2.73	2.72	2.64	2.68	2.70	2.71	2.70	2.71	2.69 ± 0.02	2.70 ± 0.03
Cu_1-S (C618)	2.48	2.46	2.39	2.41	2.43	2.45	2.43	2.37	2.36	2.37	2.43	2.47	2.42	2.46	2.45 ± 0.03	2.42 ± 0.04
Cu_1-S (C622)	2.53	2.57	2.45	2.50	2.57	2.58	2.55	2.52	2.49	2.48	2.54	2.58	2.55	2.68	2.56 ± 0.03	2.54 ± 0.07
Cu_1-S (M629)	2.43	2.38	2.49	2.42	2.44	2.51	2.50	2.37	2.45	2.48	2.52	2.42	2.48	2.43	2.47 ± 0.04	2.45 ± 0.05
Cu_1-N_δ (H583)	2.51				2.33	2.46							2.82		2.53 ± 0.09	
Cu_1-C_δ (H583)		3.46	3.49	3.84			3.93	3.86	3.69	3.68	3.47	3.85		3.29		3.66 ± 0.22

[a] H583 falls into two conformations; 'on' indicates H583 is a ligand of Cu_A site, and 'off' indicates it's too far to be a ligand.

References:

1. C. Li, A. Wen, B. Shen, J. Lu, Y. Huang and Y. Chang, *BMC Biotechnol*, 2011, **11**, 92.
2. L. Zhang, A. Wüst, B. Prasser, C. Müller and O. Einsle, *Proc. Natl. Acad. Sci. USA*, 2019, **116**, 12822-12827.
3. B. Miroux and J. E. Walker, *J. Mol. Biol.*, 1996, **260**, 289-298.
4. P. K. Smith, R. I. Krohn, G. T. Hermanson, A. K. Mallia, F. H. Gartner, M. D. Provenzano, E. K. Fujimoto, N. M. Goeke, B. J. Olson and D. C. Klenk, *Anal. Biochem.*, 1985, **150**, 76-85.
5. J. K. Kristjansson and T. C. Hollocher, *J. Biol. Chem.*, 1980, **255**, 704-707.
6. R. F. Weiss and B. A. Price, *Mar. Chem.*, 1980, **8**, 347-359.
7. A. Chaikuad, S. Knapp and F. von Delft, *Acta Crystallogr D Biol Crystallogr*, 2015, **71**, 1627-1639.
8. C. Vonrhein, C. Flensburg, P. Keller, A. Sharff, O. Smart, W. Paciorek, T. Womack and G. Bricogne, *Acta Crystallographica Section D: Biological Crystallography*, 2011, **67**, 293-302.
9. A. J. McCoy, R. W. Grosse-Kunstleve, P. D. Adams, M. D. Winn, L. C. Storoni and R. J. Read, *J. Appl. Crystallogr.*, 2007, **40**, 658-674.
10. A. Pomowski, W. G. Zumft, P. M. H. Kroneck and O. Einsle, *Nature*, 2011, **477**, 234-237.
11. G. N. Murshudov, P. Skubak, A. A. Lebedev, N. S. Pannu, R. A. Steiner, R. A. Nicholls, M. D. Winn, F. Long and A. A. Vagin, *Acta Crystallographica Section D: Biological Crystallography*, 2011, **67**, 355-367.
12. P. V. Afonine, R. W. Grosse-Kunstleve, N. Echols, J. J. Headd, N. W. Moriarty, M. Mustyakimov, T. C. Terwilliger, A. Urzhumtsev, P. H. Zwart and P. D. Adams, *Acta Crystallogr D*, 2012, **68**, 352-367.
13. P. Emsley and K. Cowtan, *Acta Crystallographica Section D: Biological Crystallography*, 2004, **60**, 2126-2132.
14. V. B. Chen, W. B. Arendall, 3rd, J. J. Headd, D. A. Keedy, R. M. Immormino, G. J. Kapral, L. W. Murray, J. S. Richardson and D. C. Richardson, *Acta Crystallographica Section D: Biological Crystallography*, 2010, **66**, 12-21.
15. L. K. Schneider and O. Einsle, *Biochemistry*, 2016, **55**, 1433-1440.
16. A. Pomowski, W. G. Zumft, P. M. Kroneck and O. Einsle, *Nature*, 2011, **477**, 234-237.